Soft Matter

Soft Matter

www.rsc.org/softmatter

ROYAL SOCIETY OF CHEMISTRY

ROYAL SOCIETY OF CHEMISTRY

www.rsc.org/softmatter

307x247mm (300 x 300 DPI)

The structure of native squid pen was investigated combining microscopy, atomic force microscopy, and X-ray diffraction. The experiments probed length scales from millimetres down to nanometres and indicate a strong correlation between macroscale structure and molecular orientation.

Hierarchical, Self-Similar Structure in Native Squid Pen

Fei-Chi Yang,[1] Robert Peters,[1] Hannah Dies,[1] and Maikel C. Rheinstädter[1, 2, *]

[1]*Department of Physics and Astronomy, McMaster University, Hamilton, ON, Canada*
[2]*Canadian Neutron Beam Centre, Chalk River, ON, Canada*
(Dated: May 19, 2014)

The structure of native squid pen (gladius) was investigated in two different species on different length scales. By combining microscopy, atomic force microscopy (AFM), and X-ray diffraction, the experiments probed length scales from millimetres down to nanometres. The gladii showed a hierarchical, self-similar structure in the optical experiments with fibres of different size oriented along the long axis of the gladius. The fibre-like structure was reproduced on the nanoscale in AFM measurements and fibres with diameters of 500 μm, 100 μm, 10 μm, 2 μm and 0.2 μm were observed. Their molecular structure was determined using X-ray diffraction. In squid gladius, the chitin molecules are known to form nano-crystallites of monoclinic lattice symmetry wrapped in a protein layer, resulting in β-chitin nano-fibrils. Signals corresponding to the α-coil protein phase and β-chitin crystallites were observed in the X-ray experiments and their orientation with respect to the fibre-axis was determined. The size of a nano-fibril was estimated from the X-ray experiments to be about 150×300 Å. About 100 of these nano-fibrils are needed to form a 0.2 μm thick micro-fibre. We find that the molecular structure is highly anisotropic with ∼90% of the α-coils and β-chitin crystallites oriented along the fibre-axis indicating a strong correlation between macroscale structure and molecular orientation.

Keywords: squid pen, squid gladius, chitin, atomic force microscopy, microscopy, molecular structure, X-ray diffraction, α-coils, monoclinic β-chitin, nano-fibrils, fibres, hierarchical organization, self-similar structure
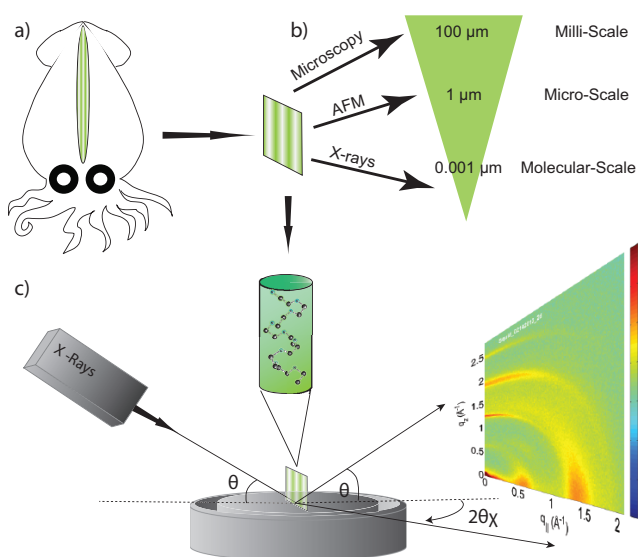
1. INTRODUCTION

FIG. 1. a) The pen (gladius) is a feather-shaped internal structure that supports the squid's mantle and serves as a site for muscle attachment. b) The structure of the gladius was studied using three different techniques: light microscopy, atomic force microscopy and X-ray diffraction, covering length scales from millimetres to the molecular level. c) By aligning the gladius, the molecular structure along the fibres and perpendicular to the fibres was studied using X-ray diffraction.

Chitin is a polymer of un-branched chains of β-(1-4)- linked 2-acetamido-2-deoxy-D-glucose (N-acetyl-Dglucosamine)[1–10]. It is widely distributed in nature, especially in marine invertebrates, insects, fungi and yeast[11,12]. Chitin occurs naturally in the crystalline state and X-ray diffraction studies of diverse supporting structures indicate three different types of crystallographic patterns among chitin[12–14]. α-chitin, whose chains are arranged in an antiparallel direction with strong intermolecular hydrogen bonding, are found in Crustacea[15]. For γ-chitin, found in the thick cuticle of the stomach of squid genus *Loligo*, the central chain is arranged in an antiparallel direction between the two adjacent ones[13,16]. In association with proteins, chitin from squid gladii forms β-chitin, a monoclinic structure where its chains are arranged in a parallel direction with relatively weak intermolecular interactions[17–19].

The gladius is a feather-shaped internal structure that supports the squid's mantle and serves as a site for muscle attachment, as sketched in Figure 1 a). Upon examination, the gladius shows a corrugated, fibre-like structure with channels running along the long axis of the squid. In addition, smaller fibres are observed on the surface of the larger, primary fibres. We combined light microscopy, atomic force microscopy (AFM), and X-ray diffraction to investigate the gladius' structure on different length scales, ranging from millimetres down to nanometres, as depicted in Figure 1 b). Hierarchical, self-similar fibre-like structures were observed on all length scales down to the molecular level. We found that ∼90% of the α-helical coils and monoclinic β-chitin crystallites were oriented parallel to the fibres indicating a correlation between structure observed on nano, micro and macroscale, and molecular orientation.

2. MATERIALS AND METHODS

2.1. Sample Preparation

Fresh squid gladii were obtained from the local fish market in Tainan, Taiwan, and in Toronto, Canada. The gladii were washed thoroughly with tap water to remove soluble organics and adherent protein and dried at room temperature in a desiccator in a magnesium nitrate atmosphere ($Mg(NO_3)_2$) at 25°C) in 52.9±0.22% relative humidity (RH). The gladii were found to deform during the drying process. In order to obtain flat pieces, the gladius was dried between two aluminum sheets. The squid gladii were cut into ∼20 mm × 10 mm pieces, optimized for the microscopy, AFM and X-ray experiments. All samples were stored in a desiccator under 52.9±0.22% RH. Details of the samples are listed in Table 1.

We note that the freshly cut gladius started to dry quickly in air, such that initial experiments did not give conclusive results as the structure kept changing during the time of the experiments. The gladii also changed when stored or investigated in ultrapure water, buffer or in salted ultrapure water due to the concentration differences. The gladii were, therefore, extracted and dried quickly in a $Mg(NO_3)_2$ atmosphere to best preserve their structure. The structure of the gladii, the surface structure as determined by AFM, and the bulk structure as determined by X-ray diffraction, could then be stabilized over several days.

The reason for the low number of species (N=2) is the availability of samples and in particular the identification of the correct species. Several squids were acquired for this project. However, the authentication of squid species is an ongoing field of research (see, e.g.,[20]). The two specimens in our study were selected based on an unambiguous identification. We note that even specimens acquired through the same provider often belong to different families. We, therefore, limit the discussion to these two specimens.

2.2. Inverted Light Microscope

Optical microscopy in this study was performed using an Olympus BX51 microscope. Samples were placed onto Silicon wafers and imaged in dark field reflection mode with a CCD camera (QIClick, QImaging), which provided high resolution images (1392 × 1040 pixels) for subsequent image analysis. In dark field microscopy, the unscattered beam is excluded from the image by illuminating the sample with light that when reflected will not be collected by the objective lens. Using this technique, increased contrast is obtained for the features in the squid gladius. A 50× magnification objective (UM-PlanFI, Olympus) was used to obtain images with a resolution of 130 nm/pixel. Additional images with lower resolution were taken using a Nikon P520 digital camera
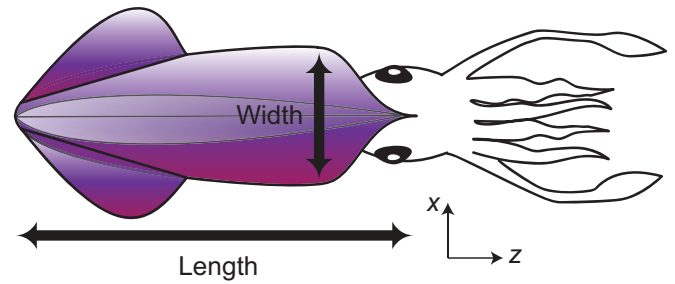
Sample	Species	length × width	gladius
1	*Sepioteuthis lessoniana*	170 mm × 150 mm	180 mm × 20 mm
2	*Uroteuthis chinensis*	255 mm × 60 mm	240 mm × 40 mm

TABLE 1. Dimensions of the two squid specimen studied. The gladius was extracted and cut into ∼20 mm × 10 mm pieces, optimized for the microscopy, AFM and X-ray experiments. All samples were stored in a desiccator under 52.9±0.22% RH at T=25°C.

in high-resolution macro setting mode.

2.3. Atomic Force Microscope

AFM was performed in constant amplitude tapping mode using a commercial AFM (Veeco Caliber, USA). The AFM was resting on an anti-vibration table on top of a granite block to provide isolation from background noise. Cantilevers with a spring constant of ∼48 N/m and a resonance frequency of 190 kHz were used for this study. Topography and tapping amplitude data were recorded simultaneously for samples mounted on Si wafers. Samples were measured at 25°C and a relative humidity of 52.9±0.22%. The humidity was controlled by sealing the AFM heads in a container with a saturated salt solution of Magnesium nitrate ($Mg(NO_3)_2$) at 25°C. Topography imaging provided a 2-dimensional map of film height in the region of interest. Similarly, tapping amplitude data offers the derivative of the topography, indicating where film height changes rapidly, clearly distinguishing the edges of squid gladius fibres.

2.4. X-ray Diffraction Experiment

X-ray diffraction data was obtained using the Biological Large Angle Diffraction Experiment (BLADE) in the Laboratory for Membrane and Protein Dynamics at McMaster University. BLADE uses a 9 kW (45 kV, 200 mA) CuKα Rigaku Smartlab rotating anode at a wavelength of 1.5418 Å. Focussing multi-layer optics provides a high intensity parallel beam with monochromatic X-ray intensities up to 10^{10} counts/(s×mm^2). A sketch of the scattering geometry is shown in Figure 1 c). By aligning the gladius in the X-ray diffractometer, the molecular structure along the fibre direction and perpendicular to the fibres could be determined. We refer to these components of the total scattering vector, Q, as q_z and $q_{||}$,

	digital camera	microscope	AFM	observed fibre size
①	×			500 μm
②	×	×		100 μm
③		×		10 μm
④		×	×	2 μm
⑤			×	0.2 μm

TABLE 2. Observed fibre sizes from the images in Figure 2. Fibres from 500 μm (①) to 0.2 μm (⑤) were observed by a digital camera, a microscope and an atomic force microscope.

respectively, in the following. The result of an X-ray experiment is a 2-dimensional intensity map of a large area of the reciprocal space of -2.5 Å^{-1} < q_z <2.5 Å^{-1} and -2 Å^{-1} < $q_{||}$ <2 Å^{-1}. The corresponding real-space length scales are determined by $d = 2\pi/|Q|$ and cover length scales from about 2.5 to 60 Å, incorporating typical molecular dimensions and distances. The squid gladius samples were kept in a temperature and humidity controlled chamber, a so-called humidity chamber, during the measurements. Data were collected at $T = 25°$C and 52.9±0.22% relative humidity by exposing them to a saturated salt solution of magnesium nitrate.

3. RESULTS

3.5. Topology from Visual Inspection, Microscopy and Atomic Force Microscopy

8 The gladii show a corrugated, rippled structure when examined by eye, as depicted in Figure 2 a). The observed fibres were well oriented running along the long axis of the squid, denoted as the z-axis in Table 1. Smaller ripples were observed on the surface of the larger, primary ripples. The higher resolution microscope image in Figure 2 b) shows a similar picture: large ripples running along the z-axis coexisting with smaller ripples. Parallel ripples and channels were also observed with submicrometre resolution in the AFM images in Figure 2 c) and d).

The sizes of the different fibres, as determined from the images in in Figure 2, are listed in Table 2. The largest fibres in Figure 2 a) have a diameter of 500 μm; smaller fibres with 100 μm were observed on top of the larger fibres. Fibres with diameters of 100 μm, 10 μm and 2 μm were observed in the dark field microscope images in Figure 2 b). 2 μm and 0.2 μm fibres were visible in the high resolution AFM images in Figures 2 c) and d).

The images in Figure 2 cover three orders of magnitude in length scale and show a hierarchical, self-similar topology of the squid gladius. With the help of X-ray diffraction measurements, we can extend the accessible length scale to the molecular scale.
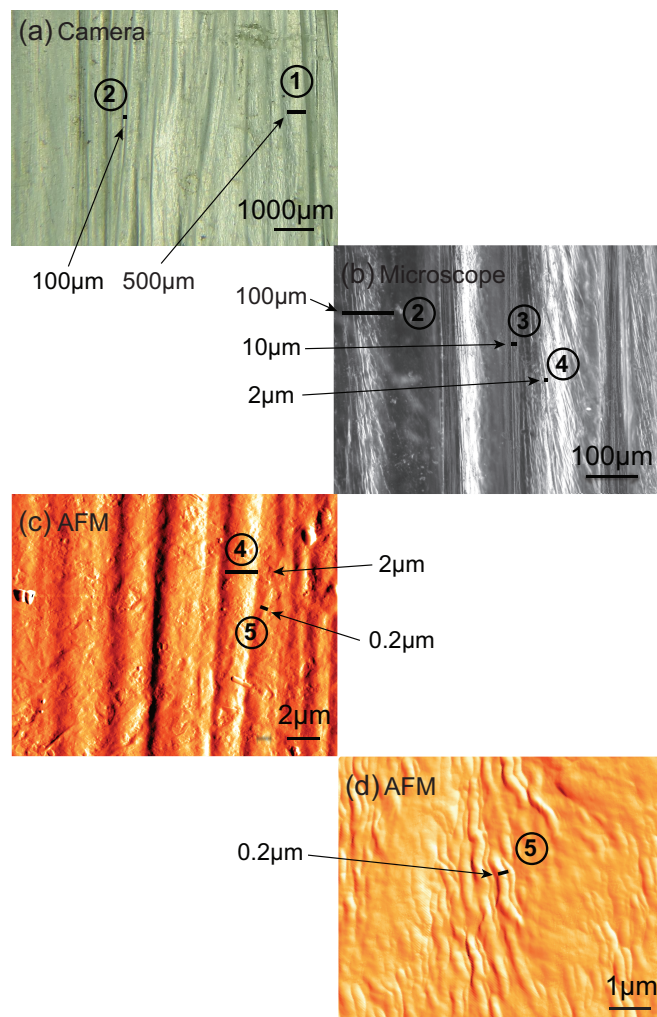

FIG. 2. The surface structure of the native squid gladii was studied using different techniques. a) Using a high resolution digital camera. b) A light microscope in dark field reflection mode and c) an AFM tapping amplitude image. d) An AFM image of the layer inside the squid gladius. The images cover length scales from millimetres down to about 100 nanometres. Self-similar, fibre-like hierarchical structures were observed on all length scales. The observed fibre sizes are listed in Table 2.

3.6. Molecular Structure from X-ray Diffraction

Figure 3 depicts 2-dimensional X-ray data of Samples 1 and 2. The displayed range was determined to cover the length scales of the features of interest in preliminary experiments. The scattered intensity in a small rectangle located at q_z ~2.25 Å^{-1} and $q_{||}$ ~2 Å^{-1}, where no diffraction maxima occurred, was used as background and subtracted from the data. The data in Figures 3 a) and b) show a distinct non-isotropic distribution of the diffracted intensity with pronounced and well defined intensities along the q_z and $q_{||}$-axes. Sample 1 was found to overall diffract less well, as checked with several pieces from different parts of the gladius, however the diffraction patterns of Samples 1 and 2 qualitatively agree very
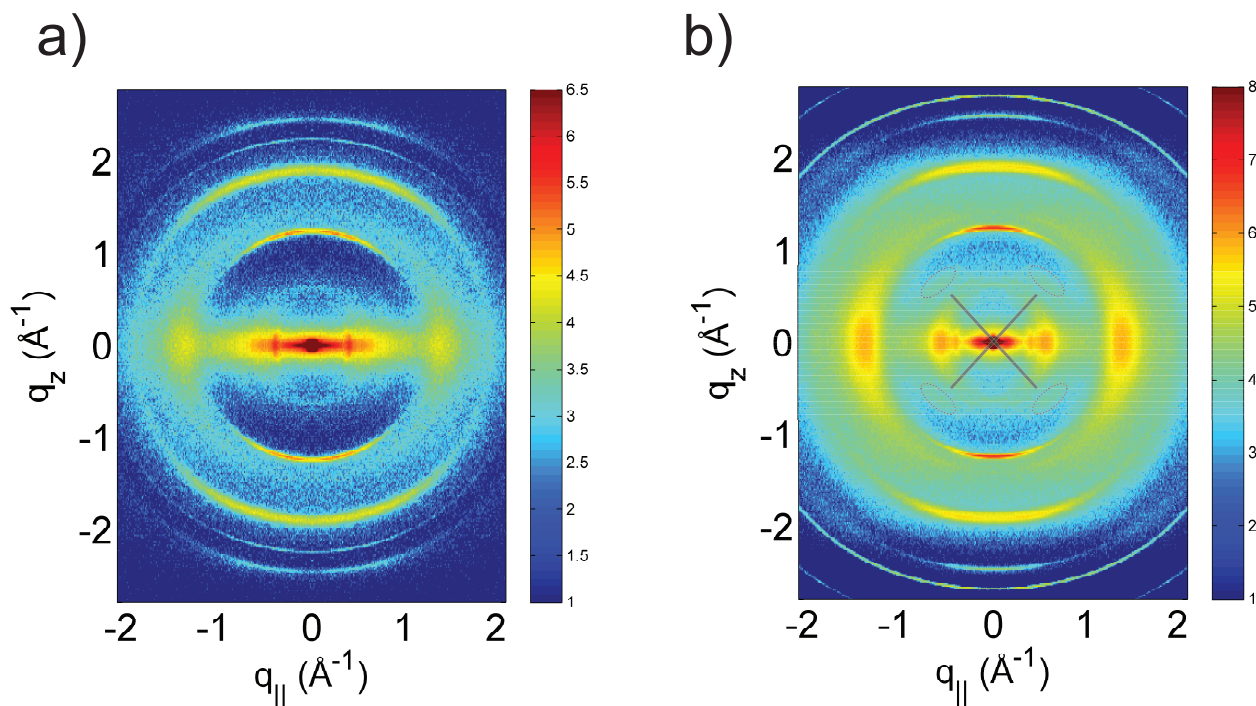
a)

b)

FIG. 3. Two-dimensional X-ray data with background subtracted for Samples 1 (a) and 2 (b). Pronounced diffraction peaks were observed along both, the q_z and $q_{||}$-axis. The fact that intensity maxima mainly occurred on one of the axis was indicative that the corresponding molecular structures are anisotropic and highly aligned with respect to z and x.

well and show the same features.

For a quantitative analysis, the 2-dimensional data were extracted and analyzed separately along the q_z and $q_{||}$-axis. The results are shown in Figures 4 a) and b). To capture all diffracted intensity of a given peak, the 2-dimensional data were integrated radially over 25° from the equator for $q_{||}$ and over 25° from the meridian for q_z, as depicted in the insets to Figures 4 a) and b). Several intensity maxima in the 1-dimensional data were observed along both the q_z and $q_{||}$-axis. Lorentzian peak profiles were fitted to and the corresponding correlations peaks labeled $1_{||}, 2_{||}, 3_{||}, 4_{||}$ and $1_z, 2_z, 3_z, 4_z$, respectively.

The angular distribution of the diffracted intensities was determined by integrating over the azimuthal angle ϕ. The corresponding ϕ-profiles of the in-plane reflections $2_{||}$ and $(3_{||} + 4_{||})$ are shown in Figure 5 a) and b). The in-plane peaks showed a broad distribution, which was well fit by a single Lorentzian peak profile with a ϕ-width (HWHM) of $\sim$17°.

Because of this large angular distribution of the diffracted intensities around equator and meridian, features could appear simultaneously in both directions in the data in Figures 4 a) and b). The peak patterns were, therefore, fitted simultaneously in q_z and $q_{||}$ using the following procedure: In a first round, the main peaks (marked as $1_{||}, 2_{||}, 3_{||}, 4_{||}$ in Figure 4 a)) were fitted in $q_{||}$. The corresponding peaks were then included in the fitting of the q_z data in Figure 4 b). Position and width were kept fixed and only the amplitude was allowed to

vary. The fitted out-of-plane Bragg peaks $1_z, 2_z, 3_z$ and 4_z were then included in fitting the $q_{||}$-axis data. This cycle was repeated several times until a good agreement between the fit and the data was obtained.

The peaks could be assigned to in-plane and out-of-plane features using this procedure, as listed in Tables 3 (in-plane) and 4 (along the fibre axis). We can at this point not assign the yellow contribution in Figures 4 a) and b), which had an identical intensity in both directions, indicative of an amorphous structure in the native gladii with a length scale of $\sim$3.8 Å. Peak $1_{||}$ stems from the Kapton windows of the X-ray humidity chamber and was, therefore, not included in the structure determination. We note that the Kapton does not scatter isotropically, which would be observed as a powder ring in the 2-dimensional diffraction data. The Kapton foils used for the X-ray windows are rolled to a thickness of 13 μm. This process leads to a preferred orientation in the polyimide film and to the observed anisotropy. The peaks in Tables 3 and 4 can be assigned to α-helical and monoclinic structures, as will be explained in the next section.

3.7. Chitin and Protein Structures in Native Squid Gladius

β-chitin is found to form in squid gladius in association with proteins[12,19,21,22]. The chitin molecules were found to organize in chitin nano-crystals, which are wrapped in a protein layer to form nano-fibrils. These fibrils even-
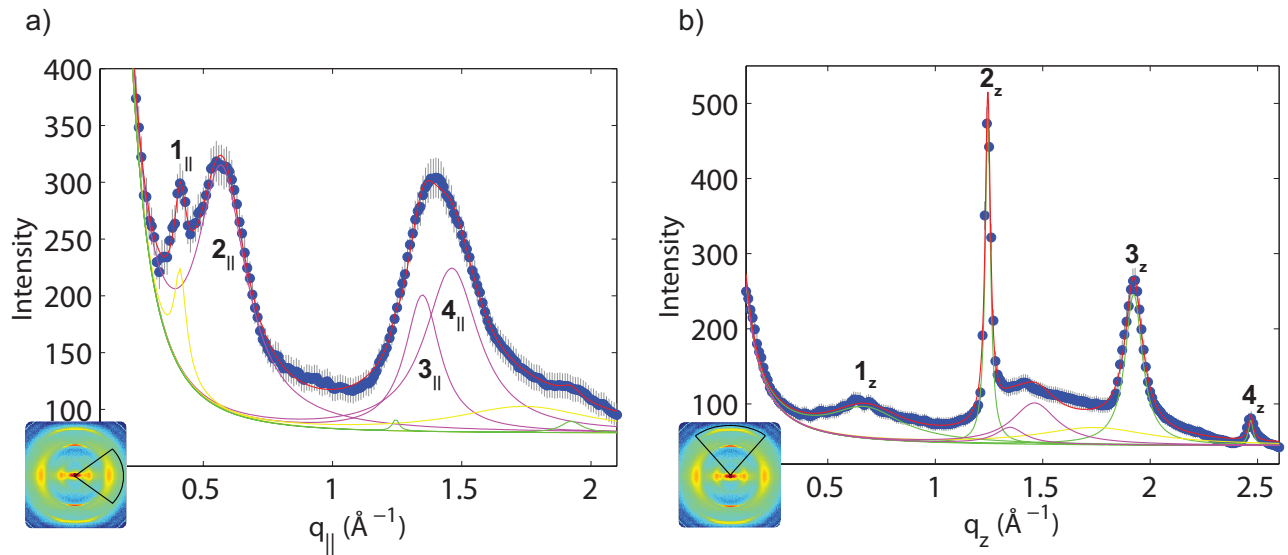
FIG. 4. The 2-dimensional data in Figure 3 were cut along the $q_{||}$ (a) and q_z-axis (b). To capture all diffracted intensity, the 2-dimensional data were integrated radially over $25°$ from the equator for $q_{||}$ and over $25°$ from the meridian for q_z, as depicted in the insets. Solid lines are fits using Lorentzian peak profiles. In-plane peaks are plotted in magenta, peaks along q_z in green. Both directions were fitted simultaneously. The fitted peak positions and widths (given as HWHM) are listed in Tables 3 and 4, and were assigned to an α-helical and a monoclinic structure.

	Sample 1			Sample 2			α-coil	monoclinic
	Amplitude (counts)	Position (Å^{-1})	Width (Å^{-1})	Amplitude (counts)	Position (Å^{-1})	Width (Å^{-1})	hkl	hkl
$1_{||}$	63±3	0.409±0.001	0.026±0.002	215±3	0.41±0.002	0.03±0.003	Kapton window	
$2_{||}$	33±2	0.58±0.01	0.21±0.02	215±3	0.571±0.002	0.115±0.004	(100)	–
$3_{||}$	15±12	1.36±0.02	0.09±0.05	120±37	1.348±0.009	0.08±0.02	–	(020)
$4_{||}$	20±10	1.48±0.06	0.16±0.05	144±38	1.46±0.02	0.13±0.03	–	(110)

TABLE 3. Fitted peak positions and widths (as HWHM) for the parallel direction in Figure 4 a). Errors given are the fitting errors. The corresponding correlation peaks were assigned to α-helical and monoclinic structures, as explained in the text.
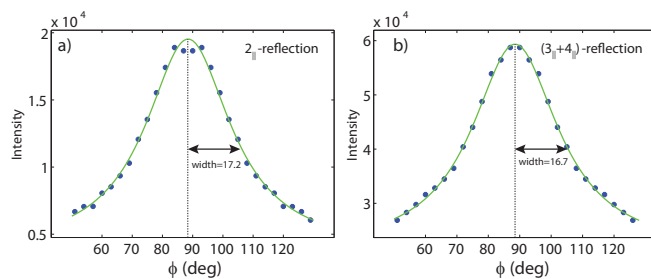

FIG. 5. The angular distributions of the diffracted intensity of the in-plane peaks (a): $2_{||}$ and (b): $\left(3_{||} + 4_{||}\right)$ could be fitted by single Lorentzians with a HWHM of $\sim17°$.

tually organize into larger fibres. When extracting β-chitin from squid gladius, yields between $\sim$25-45% were reported[19,22]. The protein component after chemical extraction is typically $\sim$75%. The X-ray experiments were sensitive to the corresponding protein and chitin structures, namely the α-helical protein phase and the monoclinic β-chitin crystallites.

3.8. Scattering from α-Coils

The diffraction pattern of an ideal helix was first written down by Pauling and Corey[23]. The periodic structures of the helix along the diagonal directions are the well-known helix peaks, which typically appear as a cross in X-ray diffraction experiments in crystalline, well-ordered specimen[24–26]. The first order helix peak is observed as a weak feature in the 2-dimensional data in Figure 3, as marked by the circle. Higher order peaks and side oscillations are usually observed in crystalline specimen measured at liquid nitrogen temperature. They are, however, most likely suppressed by thermal positional fluctuations and the intrinsic disorder in native samples at elevated temperatures. The $q_{||}$ and q_z position of the helical peak can map to the distance of the pitch, P_h, of the helices and the radius, R_h, in real space by: $q_{||} = 5\pi/(8R_h)$ and $q_z = 2\pi/P_h$. The position of the (101) peak of the helices are found to be $q_{||}$=0.60 Å^{-1} and q_z=0.60 Å^{-1} for Sample 1 and $q_{||}$=0.53 Å^{-1} and $q_{||}$=0.80 Å^{-1} for Sample 2. The values for R_h and P_h for both samples were calculated using the above equations and are listed in Table 5.

	Sample 1			Sample 2			α-coil	monoclinic
	Amplitude (counts)	Position (Å⁻¹)	Width (Å⁻¹)	Amplitude (counts)	Position (Å⁻¹)	Width (Å⁻¹)	hkl	hkl
1_z	9.6±0.6	0.619±0.007	0.12±0.01	42±3	0.68±0.01	0.21±0.02	–	(001)
2_z	122±3	1.2439±0.0004	0.0166±0.0005	433±18	1.2447±0.0005	0.0149±0.0007	(001)	(002)
3_z	66±1	1.9098±0.0009	0.0550±0.0001	200±7	1.924±0.002	0.049±0.002	–	(003)
4_z	165±1	2.473±0.002	0.044±0.004	33±8	2.469±0.003	0.014±0.005	–	(004)

TABLE 4. Fitted peak positions and widths (as HWHM) for the perpendicular direction in Figure 4 b). Errors given are the fitting errors. The corresponding correlation peaks were assigned to α-helical and monoclinic structures.

The proteins in squid gladius are known to organize in bundles of proteins, whose structure is dominated by α-helical coiled-coils. The main features of this pattern is a ∼10 Å (corresponding to $q_{||}$ ∼0.6 Å^{-1}) equatorial reflection corresponding to the spacing between adjacent coiled-coils and a ∼5.0 Å meridional reflection (corresponding to q_z ∼1.25 Å^{-1}) corresponding to the superhelical structure of α-helices twisting around each other within coiled-coils[27–29]. Reflections $2_{||}$ and 2_z in Tables 3 and 4 were, therefore, assigned to α-coil structures. We note that these peaks are related to generic α-helical coil structures of monomeric proteins, and not specific a to certain type of protein. Because helix and coiled-coil peaks were found in the diffraction data, we argue that these peaks belong to a protein phase rather than for instance α-chitin.

3.9. Scattering from β-Chitin

Crystalline monoclinic β-chitin was reported to order in the monoclinic space group $P2_1$ with unit cell dimensions a=4.85 Å, b=9.26 Å c=10.38 Å and β=97.5° by Blackwell, Parker and Rudall.[17,18] The corresponding q_{hkl}-positions for a monoclinic symmetry are given by[30]:

$$q_{hkl}^2 = \frac{4\pi^2}{\sin^2\gamma}\left(\frac{h^2}{a^2} + \frac{k^2}{b^2} + \frac{l^2\sin^2\gamma}{c^2} - \frac{2hk\cos\gamma}{ab}\right) \quad (1)$$

The position of the (020), (110), (001), (002), (003), (004) reflections agree well with the reported monoclinic β-chitin structure. One thing worth noting is that the (001) and (003) reflections, which should be systematic absent in this space group, were observed in the data. This effect is frequently observed in soft materials and a consequence of the inherent disorder in these systems[31,32]. Extinction rules may be lifted when soft structures deviate from their nominal crystal structure to form a space filling pattern.

The lattice parameters were determined from the $q_{z/||}$-values in Tables 3 and 4. The monoclinic angle, γ, could not be determined from our measurements, as only powder averages were observed the ab-plane (perpendicular to the fibre-axis) in native gladius. As a result, the value of γ=97.5° was used from the original papers by Blackwell[17,18]. The lattice parameter c was determined from the averaged positions of the (001) reflection:

$$q_{(001)}^2 = \left(\frac{4\pi^2 1^2}{c^2}\right) \quad (2)$$

to be c=10.15 Å. Parameters a and b were determined from the positions of the (020) and (110) peaks along the $q_{||}$-axis:

$$q_{(020)}^2 = \frac{4\pi^2}{\sin^2\gamma}\left(\frac{2^2}{b^2}\right) \quad (3)$$

and

$$q_{(110)}^2 = \frac{4\pi^2}{\sin^2\gamma}\left(\frac{1^2}{a^2} + \frac{1^2}{b^2} - \frac{2\cdot1\cdot1\cos\gamma}{ab}\right) \quad (4)$$

to a=9.32 Å and b=5.15 Å. The monoclinic unit cell parameters for the two samples are listed in Table 4.

We note that the 2_z reflection in Figure 4 b) is significantly stronger than the other reflections. Based on the models above, this peak has contributions from both the coiled-coils and the monoclinic lattice.

4. DISCUSSION

A hierarchical chitin structure was found in crustacean exoskeleton[33,34], where fibres consisting of α-chitin crystals organize into a planar woven and periodically branched network in a so-called twisted plywood structure of high stiffness. Concerning β-chitin, a periodic structure in the gladius of the squid *Loligo vulgaris* was observed by Hunt and Sherief[35] using electron microscopy and was related to the formation of chitin/protein complexes. Corresponding protein-chitin structures were reported decades ago by Blackwell, Germinario and Weih[21], where the proteins formed a helical sheath around chitin fibrils. A lamellar structure was also reported more recently by Lavall, Assis and Campana-Filho[22]. De-proteinated, de-mineralized and de-acetylated gladii were used for these studies. We studied the molecular structure and organization in the native state of the gladius.

We observed a hierarchical, self-similar structure in the gladius of two different species. The surface of the gladii showed a fibre-like structure with fibres running along the long axis of the squid by eye, under the light microscope and the AFM. The diffracted intensities in the X-ray experiments could be assigned to an α-helical protein phase and monoclinic β-chitin crystallites. The corresponding lattice parameters in Table 5 are in good agreement with the parameters for crystalline β-chitin, as determined by Blackwell[17,18]. The absolute values for the monoclinic

parameters a, b and c deviate by $\sim$7% from Blackwell's values. The largest deviation was observed in the lattice parameter a. Because it was not possible to determine the monoclinic angle, γ, independently from our X-ray measurements, this difference could also be the result of a slightly different γ-value. We note that the differences in the lattice parameters between the two species, which were investigated in this study, were much smaller, namely less than 3%.

Herman's orientation function,

$$f = \frac{3 < \cos^2(\phi) > -1}{2}, \qquad (5)$$

was used to determine the degree of orientation of the α-coils and monoclinic β-chitin crystallites with respect to the fibre-axis. The ϕ (azimuthal) profiles are plotted and fitted in Figures 5 a) and b). The angular width of the peak $2_{||}$ in Figure 5 a) was used to obtain the orientation of the α-coils. The reflections $(3_{||} + 4_{||})$ in Figure 5 b) determined the orientation of the β-chitin crystallites. Using the above equation, 92% of the β-chitin crystallites and α-coils in Sample 2 were oriented along the fibre (z) axis of the squid gladii. The values are summarized in Table 5.

The results of the X-ray diffraction experiments indicate a high degree of molecular organization in native squid gladius. These results strongly support the results of Blackwell[21], who suggested chitin fibrils wrapped in helical proteins as the elementary unit of organization. From the X-ray data in Figure 3 and Table 5, these complexes were found to be highly aligned along the long axis of the gladii. The self-similar structures, which were observed on different length scales in Figure 2, suggest that these fibrils organize in larger and larger fibres, which eventually result in the corrugated macroscopic structure.

We note that while the distribution of the $2_{||}$ reflection in Figure 5 a) is well fitted by a Lorentzian peak profile, the top of the peak appears to be slightly split. A splitting of the 2_z peak can also be observed in the 2-dimensional data in Figure 3 a). Peaks 1_z, 2_z, 3_z and 4_z can be assigned to the monoclinic β-chitin phase. If the observed splitting was related to β-chitin, it should be more pronounced in the higher order reflections 3_z and 4_z. The absence of a splitting in these peaks is strong evidence that the observed effect is due to the (001) reflection of the α-coil phase. Following the same argument, the $2_{||}$ reflection is part of the α-coil phase; peaks $3_{||}$ and $4_{||}$ are related to the β-chitin phase. The split is, therefore, indicative of a preferred tilt of $\sim$10° of the α-coils in the coiled-coil phase with respect to the z-axis of the gladius.

The size of the β-chitin crystallites and the coiled-coil phase was estimated by applying Scherrer's equation[36]:

$$L = \frac{0.94\lambda}{B(2\theta)cos(\theta)}, \qquad (6)$$

where λ is the wavelength of the X-ray beam, θ is the

diffraction angle and $B(2\theta)$ is the width of the correlation peak in radians. Using the parameters in Tables 3 and 4 for the $2_{||}$ and $3_{||}$-reflections for coil phase and β-chitin, respectively, the size of the corresponding protein phase and the β-chitin crystallites can be calculated. The corresponding values are listed in Table 5.

A protein layer of 51 Å is calculated for Sample 2 and a crystallite size of $\sim$74 Å. When assuming that a nano-fibril is composed of one crystallite wrapped in a protein layer, the diameter of such a nano-fibril can be estimated by the size of a crystallite and two layers of proteins to $\sim$176 Å. This value is in good agreement with Mulisch et al.[37], who reported $\sim$20 nm wide fibrils. From the width of the correlation peak in z-direction, the length of a nano-fibril can be estimated to 324 Å, based on a crystallite length of 222 Å and two protein layers. The findings are summarized in Figure 6.

The smallest fibre (a micro-fibre) that could be resolved in the AFM experiments in Figure 2 and Table 2 had a diameter of about 2000 Å (0.2 μm). Based on the spatial resolution of AFM and X-ray experiment we can at this point not exclude the existence of even smaller fibres whose size would be slightly too small to be resolved by the AFM, yet too large to be detected by wide-angle X-ray diffraction. However, when assuming that the nano-fibrils form a hexagonally close-packed structure, the total number of nano-fibrils in a micro-fibre can be estimated by the ratio between their areas multiplied by the packing density of close packed cylinders of 0.91 to $\sim$117 nano-fibrils.

One of the hallmarks of biological materials is their strictly hierarchical organization on different levels[12,33]. This organization is often linked to superior mechanical properties, such as high tensile strength, toughness and bending resistance[38]. The corresponding structures are typically assembled from the bottom up, rather than from the top down, and spontaneously self-assemble on the nanoscale. The fact that natural materials are growing (both the material and the whole organism grow at the same time) rather than being fabricated makes them more complex than synthetic materials[39]. Hierarchical self-assembly is often related to fractals because of their self-similarity, as recently reported for coiled-coils peptides[40] and in particular protein fibres[41,42]. The process of self-assembly is the result of a complex interplay between free energy and entropy, where order and organization eventually wins over the second law of thermodynamics[43].

5. CONCLUSIONS

The squid gladius is an internal structure that supports the squid's mantle and serves as a site for muscle attachment. It is made of two main components, proteins and β-chitin. We find evidence for a hierarchical, self-similar structure in native squid gladius from millimetres down to the molecular level. The extracted gladii showed an

Sample	α-coils				monoclinic β-chitin						nano-fibril	
	R_h (Å)	P_h (Å)	degree of orientation (f_α)	protein layer thickness (Å)	a (Å)	b (Å)	c (Å)	γ (°)	degree of orientation (f_β)	crystallite size (Å)	diameter (Å)	length (Å)
1	3.70	7.85	92.0%	28	5.15	9.32	10.15	97.5	92.3%	65 × 163	122	219
2	3.27	10.47	86.9%	51	5.24	9.40	9.24	97.5	87.5%	74 × 222	176	324

TABLE 5. Structural parameters of the α-helical coil and monoclinic β-chitin crystallites, as determined from the peak positions in Tables 3 and 4. The degree of orientation of the coils and crystallites with respect to the fibre-axis in Figure 2 was determined by Herman's orientation function. The dimension of the two structures was estimated using Scherrer's Equation. Diameter and length of the protein/chitin nano-fibrils was estimated from the protein layer thickness and the chitin crystallite size, as described in the text.
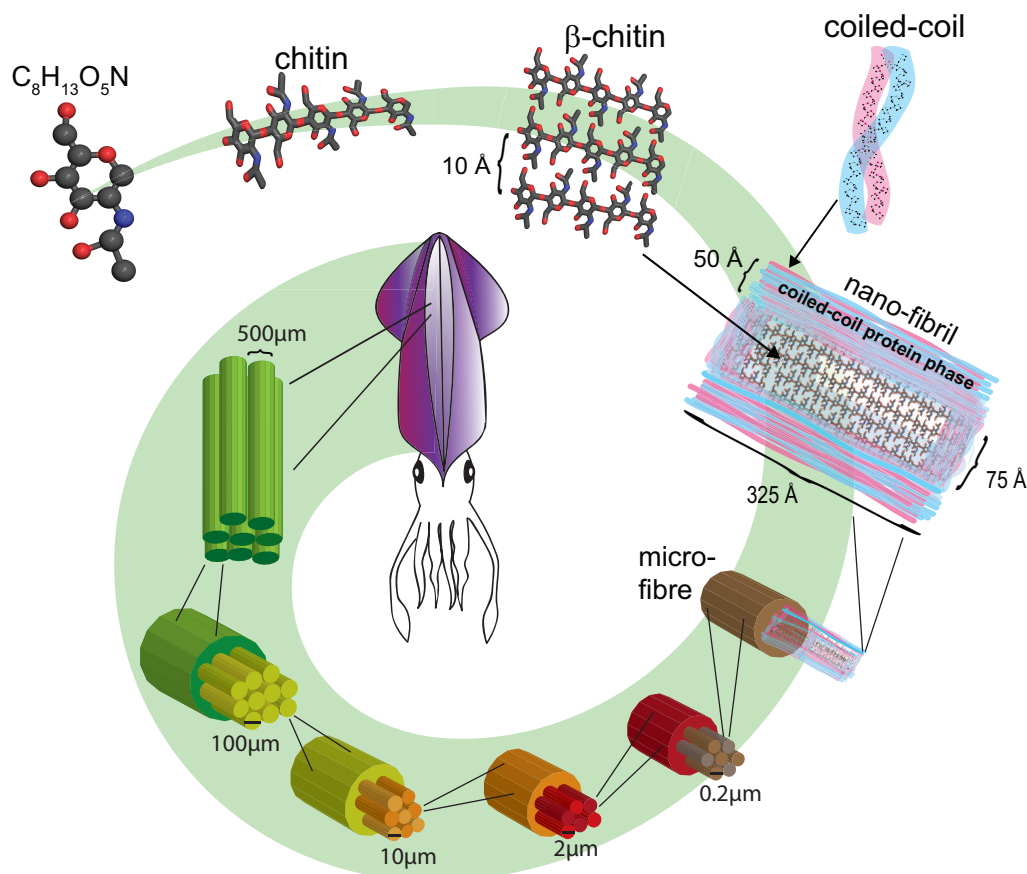

FIG. 6. Hierarchy of the main structural levels in squid gladius: β-chitin crystallites wrapped in a protein layer form so-called nano-fibrils, which are the building blocks of 0.2 μm sized micro-fibres. These fibres aggregate into 2 μm, 10 μm, 100 μm and 500 μm thick fibres, which eventually form the squid gladius.

anisotropic, fibre-like structure by eye and under the microscope. A self-similar structure was observed on the nanoscale with an AFM and fibres with diameters between 500 μm down to 0.2 μm were observed. Using X-ray diffraction, the molecular structure of native squid gladii of the two different species was determined. Scattering signals corresponding to an α-helical protein phase and the monoclinic β-chitin crystallites were observed. The chitin lattice parameters in the two species agreed well with parameters reported in the literature. About 90% of the α-coils and β-chitin crystallites were found to be oriented along the fibre axis. From the size of a β-chitin crystallite and the protein phase, the size of a nano-fibril was estimated to be ∼150 Å×300 Å. About 100 nano-fibrils then form a micro-fibre, with a diameter of 0.2 μm. The experiments present evidence for a strong correlation between macroscale structure and molecular orientation.

---

* rheinstadter@mcmaster.ca

[1] Richards AG (1951) The integument of arthropods: the chemical components and their properties, the anatomy and development, and the permeability. U of Minnesota Press.

[2] Runham N (1961) Investigations into the histochemistry of chitin. Journal of Histochemistry & Cytochemistry 9: 87-92.

[3] Rudall K (1955) The distribution of collagen and chitin in fibrous proteins and their biological significance. Sym Soc Exp Biol 9: 4971.

[4] Rudall K, Kenchington W (1973) The chitin system. Biol Rev 48: 597-636.

[5] Brown C (1975) Structural materials in animals. London: Pitman.

[6] Pont LR, Quesada-Allue L (1990) Chitin. Method Plant Biochem 2: 443-481.

[7] Giraud-Guille M, Belamie E, Mosser G (2004) Organic and mineral networks in carapaces, bones and biomimetic materials. CR Palevol 3: 503-513.

[8] Kurita K (2006) Chitin and chitosan: Functional biopolymers from marine crustaceans. Mar Biotechnol 8: 203-226.

[9] Kumar R, Muzzarelli R, Muzzarelli C, Sashiwa H, Domb A (2004) Chitosan chemistry and pharmaceutical perspectives. Chem Rev 104: 6017-6084.

[10] Aranaz I, Mengíbar M, Harris R, Paños I, Miralles B, et al. (2009) Functional characterization of chitin and chitosan. Current Chemical Biology 3: 203–230.

[11] Austin P, Brine C, Castle J, Zikakis J (1981) Chitin: New facets of research. Science 212: 749-753.

[12] Muzzarelli RA (2011) Chitin nanostructures in living organisms. Chitin, Springer, Heidelberg : 1-34.

[13] Rudall K (1963) The chitin/protein complexes of insect cuticles. Advances in Insect Physiology 1: 257 - 313.

[14] Khoushab F, Yamabhai M (2010) Chitin research revisited. Marine drugs 8: 1988–2012.

[15] Minke R, Blackwell J (1978) The structure of α-chitin. Journal of molecular biology 120: 167–181.

[16] Deshpande M (1986) Enzymatic degradation of chitin & its biological applications. Journal of Scientific and Industrial Research 45: 273-281.

[17] Blackwell J, Parker K, Rudall K (1967) Chitin fibres of the diatoms thalassiosira fluviatilis and cyclotella cryptica. Journal of Molecular Biology 28: 383 - 385.

[18] Gardner K, Blackwell J (1975) Refinement of the structure of β-chitin. Biopolymers 14: 1581–1595.

[19] Youn DK, No HK, Prinyawiwatkul W (2013) Preparation and characteristics of squid pen β-chitin prepared under optimal deproteinisation and demineralisation condition. International Journal of Food Science & Technology 48: 571–577.

[20] neira ME, Vieites JM, Santaclara FJ (2010) Species authentication of octopus, cuttlefish, bobtail and bottle squids (families octopodidae, sepiidae and sepiolidae) by {FINS} methodology in seafoods. Food Chemistry 121: 527 - 532.

[21] Blackwell J, Germinario L, Weih MA (1982) Chitinprotein complexes. Biological Activities of Polymers : 149-162.

[22] Lavall RL, Assis OB, Campana-Filho SP (2007) β-chitin from the pens of *loligo sp.*: Extraction and characterization. Bioresource technology 98: 2465–2472.

[23] Pauling L, Corey RB (1951) Atomic coordinates and structure factors for two helical configurations of polypeptide chains. Proc Natl Acad Sci USA 37: 235-240.

[24] Spaar A, Münster C, Saldit T (2004) Conformation of peptides in lipid membranes studied by x-ray grazing incidence scattering. Biophys J 87: 396-407.

[25] Schneggenburger P, Beerlink A, Weinhausen B, Salditt T, Diederichsen U (2011) Peptide model helices in lipid membranes: insertion, positioning, and lipid response on aggregation studied by x-ray scattering. European Biophysics Journal 40: 417-436.

[26] Salditt T, Li C, Spaar A (2006) Structure of antimicrobial peptides and lipid membranes probed by interface-sensitive x-ray scattering. Biochimica et Biophysica Acta (BBA) - Biomembranes 1758: 1483 - 1498.

[27] Crick F (1952) Is α-keratin a coiled coil? Nature 170: 882 - 883.

[28] Cohen C, Parry D (1994) Alpha-helical coiled coils: more facts and better predictions. Science 263: 488-489.

[29] Lupas AN, Gruber M (2005) The structure of α-helical coiled coils. Advances in protein chemistry 70: 37–38.

[30] Cullity B (1978) Elements of X-ray Diffraction. Addison-Wesley, Reading, MA,.

[31] Förster S, Timmann A, Schellbach C, Frömsdorf A, Kornowski A, et al. (2007) Order causes secondary bragg peaks in soft materials. Nature Materials 6: 888-893.

[32] Armstrong CL, Barrett MA, Toppozini L, Kučerka N, Yamani Z, et al. (2012) Co-existence of gel and fluid domains in single-component phospholipid membranes. Soft Matter 8: 4687-4694.

[33] Raabe D, Sachs C, Romano P (2005) The crustacean exoskeleton as an example of a structurally and mechanically graded biological nanocomposite material. Acta Materialia 53: 4281-4292.

[34] Raabe D, Romano P, Sachs C, Fabritius H, Al-Sawalmih A, et al. (2006) Microstructure and crystallographic texture of the chitin–protein network in the biological composite material of the exoskeleton of the lobster¡ i¿ homarus americanus¡/i¿. Materials Science and Engineering: A 421: 143–153.

[35] Hunt S, El Sherief A (1990) A periodic structure in the penchitin of the squid *loligo vulgaris*. Tissue and Cell 22: 191–197.

[36] Scherrer P (1918) Bestimmung der Größe und der inneren Struktur von Kollidteilchen mittels Röntgenstrahlen. Göttinger Nachrichten Math Phys 2: 98-100.

[37] Mulisch M, Herth W, Zugenmaier P, Hausmann K (1983) Chitin fibrils in the lorica of the ciliate eufolliculina uhligi: ultrastructure, extracellular assembly and experimental inhibition. Biology of the cell 49: 169–177.

[38] Meyers MA, McKittrick J, Chen PY (2013) Structural biological materials: Critical mechanics-materials connections. Science 339: 773-779.

[39] Fratzl P, Weinkamer R (2007) Natures hierarchical materials. Progress in Materials Science 52: 1263 - 1334.

[40] Lomander A, Hwang W, Zhang S (2005) Hierarchical self-assembly of a coiled-coil peptide into fractal structure. Nano Letters 5: 1255-1260.

[41] Murr MM, Morse DE (2005) Fractal intermediates in the self-assembly of silicatein filaments. Proceedings of the National Academy of Sciences of the United States of America 102: 11657-11662.

[42] Khire TS, Kundu J, Kundu SC, Yadavalli VK (2010) The fractal self-assembly of the silk protein sericin. Soft Matter 6: 2066-2071.

[43] Meyers MA, Chen PY, Lin AYM, Seki Y (2008) Biological materials: Structure and mechanical properties. Progress in Materials Science 53: 1 - 206.